HAL
open science

Anisotropic thermal expansion of bismuth from first principles

Brice Arnaud, Sébastien Lebègue, Guillaume Raffy

To cite this version:

Brice Arnaud, Sébastien Lebègue, Guillaume Raffy. Anisotropic thermal expansion of bismuth from first principles. Physical Review B, 2016, 93 (9), pp.094106. 10.1103/PhysRevB.93.094106 . hal-01319977

HAL Id: hal-01319977

https://univ-rennes.hal.science/hal-01319977v1

Submitted on 7 Oct 2016

HAL is a multi-disciplinary open access archive for the deposit and dissemination of scientific research documents, whether they are published or not. The documents may come from teaching and research institutions in France or abroad, or from public or private research centers.

L'archive ouverte pluridisciplinaire **HAL**, est destinée au dépôt et à la diffusion de documents scientifiques de niveau recherche, publiés ou non, émanant des établissements d'enseignement et de recherche français ou étrangers, des laboratoires publics ou privés.

Anisotropic thermal expansion of bismuth from first principles

B. Arnaud[1], S. Lebègue[2] and G. Raffy[1]

[1]*Institut de Physique de Rennes (IPR),*

UMR UR1-CNRS 6251, Campus de Beaulieu - Bat 11 A,

35042 Rennes Cedex, France, EU and

[2]*Laboratoire de Cristallographie, Résonance Magnétique et Modélisations (CRM2),*

UMR CNRS 7036, Institut Jean Barriol,

Université de Lorraine, BP 239, Boulevard des Aiguillettes,

54506 Vandoeuvre-lès-Nancy, France, EU

(Dated: February 4, 2016)

Abstract

Some anisotropy in both mechanical and thermodynamical properties of bismuth is expected. A combination of density functional theory total energy calculations and density functional perturbation theory in the local density approximation is used to compute the elastic constants at 0 K using a finite strain approach and the thermal expansion tensor in the quasiharmonic approximation. The overall agreement with experiment is good. Furthermore, the anisotropy in the thermal expansion is found to arise from the anisotropy in both the directional compressibilities and the directional Grüneisen functions.

PACS numbers: 63.20.dk, 65.40.De

Final draft post-refeering (pre-proofs)

I. INTRODUCTION

The semimetal bismuth is of interest both scientifically and technologically. Indeed, it exhibits many fascinating properties, like giant magnetoresistance[1,2], thermoelectricity[3,4], large diamagnetism[5] that can be ascribed to the peculiar electronic structure of bismuth, namely the small overlap between the valence and the conduction bands giving rise to a Fermi surface made of tiny electron and hole pockets[6]. Real-world applications of bismuth related to the aforementioned properties range from hall magnetometry[7] to diamagnetic levitation on the microscale[8].

The possibility to drive bismuth strongly out of equilibrium by an ultrashort laser pulse is also behind a huge amount of experimental[9–14] and theoretical work[15–19]. From a theoretical point of view, the ultrafast dynamics of coherent optical phonons has been tackled by means of first-principles calculations where the lattice parameters are kept constant. However, the development of strain from coherent acoustic phonons on a picosecond timescale is still poorly understood[20] and has never been addressed by ab-initio calculations. A prerequisite for achieving such a goal is to demonstrate that the thermal expansion of bismuth at equilibrium can be understood and predicted by performing ab-initio calculations. A good strategy is to resort to the quasiharmonic approximation, where the atoms of the crystal are considered to undergo harmonic oscillations, but with frequencies that depend on strain. This approximation, when combined with density functional perturbation theory[21], has been found to produce thermal expansion coefficients in good agreement with experimental results well below the melting temperature of isotropic[22–24] and anisotropic solids[25–28].

The paper is organized as follows. In section II, we give an account of the technicalities used to perform our first-principles calculations. In section III, we describe the crystallographic structure of bismuth and compare our calculated lattice constants with and without spin-orbit interaction (SOI) to the experimental lattice constants at 4 K obtained from X-ray measurements. In section IV, we explain how the elastic constants at 0 K can be computed using a finite strain method and make a comparison with available experimental results indirectly obtained by measuring the sound wave velocities for different directions and polarizations. We also discuss the impact of SOI on the calculated elastic constants. In section V, we introduce the theory allowing the calculation of the thermal expansion tensor of bismuth within the quasiharmonic approximation and compare the thermal expansion co-

Final draft post-refeering (pre-proofs)

TABLE I. Calculated LDA lattice parameters with and without SOI compared to the experimental results of Ref[32].

	Rhombohedral structure			Hexagonal structure	
	a_0 (Å)	α_0 (^{o})	V_0 (Å^3)	$a_{\parallel,0}$ (Å)	$a_{\perp,0}$ (Å)
Experiment	4.724	57.35	69.97	11.796	4.533
Theory (without SOI)	4.653	57.48	67.12	11.610	4.475
Theory (with SOI)	4.697	57.53	69.10	11.714	4.521

efficients parallel and perpendicular to the trigonal axis to some measurements made using an optical lever dilatometer. We also unravel the role respectively played by the elasticity and the anharmonicity in the anisotropy of the thermal expansion coefficients of bismuth. Finally, the specific heat at constant pressure is reported and compared with calorimetry measurements.

II. COMPUTATIONAL DETAILS

All the calculations are performed using the ABINIT code[29]. We use a plane-wave basis set, the Hartwigsen-Goedecker-Hutter (HGH) pseudopotentials[30] and the local density approximation (LDA) for the exchange-correlation functional. We carefully check the convergence of our results with respect to the wave function cut-off and the k-point sampling of the Brillouin zone. A 40 Ry cut-off and a $16 \times 16 \times 16$ mesh for Brillouin zone sampling ensure that our results (lattice parameters, elastic constants, phonon frequencies) are well converged. The dynamical matrix is explicitly calculated on a $8 \times 8 \times 8$ q-point mesh using density functional perturbation theory[31] and the phonon frequencies are Fourier interpolated on a $32 \times 32 \times 32$ q-point mesh in order to compute the thermal expansion tensor. We include SOI in all calculations but also present the lattice parameters and elastic constants obtained without SOI in order to highlight the crucial role played by SOI.

Final draft post-refeering (pre-proofs)

III. LATTICE PARAMETERS AT ZERO TEMPERATURE

Bismuth crystallizes in a rhomboedral structure, also called A7 structure, with two atoms per unit cell. The vectors spanning the unit cell are given by

$$\mathbf{a}_1 = \left(a\xi, -\frac{a\xi}{\sqrt{3}}, h\right); \mathbf{a}_2 = \left(0, \frac{2a\xi}{\sqrt{3}}, h\right); \mathbf{a}_3 = \left(-a\xi, -\frac{a\xi}{\sqrt{3}}, h\right), \tag{1}$$

where $\xi = \sin[\frac{\alpha}{2}]$ and $h = a\sqrt{1 - \frac{4}{3}\xi^2}$. The length of the three lattice vectors is equal to a and the angle between any pair of vector is α. The two atoms belonging to the unit cell are located at $\pm u\,(\mathbf{a}_1 + \mathbf{a}_2 + \mathbf{a}_3)$ where u is a dimensionless parameter and $\mathbf{a}_1 + \mathbf{a}_2 + \mathbf{a}_3$ is parallel to the ternary axis (C_3 axis). Alternatively, the structure can be viewed as an hexagonal structure spanned by the following three lattice vectors

$$\tilde{\mathbf{a}}_1 = \mathbf{a}_1 - \mathbf{a}_2;\ \tilde{\mathbf{a}}_2 = \mathbf{a}_2 - \mathbf{a}_3;\ \tilde{\mathbf{a}}_3 = \mathbf{a}_1 + \mathbf{a}_2 + \mathbf{a}_3, \tag{2}$$

where $\tilde{a}_1 = \tilde{a}_2 \equiv a_\perp$ and $\tilde{a}_3 \equiv a_\parallel$. The lattice cell parameters of the two structures are related to each other by the following relations

$$\begin{array}{ll} a_\perp = 2a\sin\left(\frac{\alpha}{2}\right) & a = \frac{1}{3}\sqrt{3a_\perp^2 + a_\parallel^2} \\ a_\parallel = a\sqrt{3 + 6\cos(\alpha)} & \sin\left[\frac{\alpha}{2}\right] = \frac{3}{2}a_\perp/\sqrt{3a_\perp^2 + a_\parallel^2} \end{array} \tag{3}$$

All the calculations have been performed using the rhombohedral structure because it contains three times atoms less than the hexagonal structure. However, the hexagonal structure, as will be seen later, is more convenient to define thermal expansion coefficients. Our calculated LDA lattice parameters with and without SOI are given in Table I along with the experimental results at 4.2 K[32]. The agreement between theory and experiment is significantly improved when SOI is included[33]. Indeed, $a_{\parallel,0}$ and $a_{\perp,0}$ are respectively underestimated from 0.69 % (1.58 %) and 0.26 % (1.27 %) with respect to experiments, leading to an underestimation of the equilibrium volume V_0 of 1.2 % (4.1 %) when SOI is included (neglected). Thus, the inclusion of SOI is mandatory to achieve a better description of the equilibrium lattice parameters of bismuth.

Final draft post-refeering (pre-proofs)

IV. ELASTIC CONSTANTS AT ZERO TEMPERATURE

The elastic properties of a bismuth crystal can be inferred from the theory of elasticity. The Lagrangian strain tensor η is defined as

$$\eta_{ab} = \epsilon_{ab} + \frac{1}{2}\sum_k \epsilon_{ak}\epsilon_{kb} \tag{4}$$

where ϵ is the linear strain tensor which transforms a vector $\mathbf{a}$ into $(\mathbf{1}+\epsilon)\mathbf{a}$. The energy of the crystal per unit cell E can be expanded in power series with respect to the strain η as

$$E[\eta] = E_0 + \frac{V_0}{2}\sum_{ijkl} C_{ijkl}\eta_{ij}\eta_{kl} + \cdots \tag{5}$$

where E_0 and V_0 are the energy and the volume of the unstrained unit cell and C_{ijkl} are the elastic stiffness constants of the crystal. Using Voigt's notation, Eq. 5 can be written as

$$E[\eta] = E_0 + \frac{V_0}{2}\sum_{\alpha\beta} C_{\alpha\beta}\eta_\alpha\eta_\beta + \cdots \tag{6}$$

where the fourth-rank stiffness tensor has been replaced by a 6×6 matrix $\mathbf{C}$. By virtue of the rhombohedral structure A7 of bismuth (space group R$\overline{3}$m), the matrix $\mathbf{C}$ can be cast in the form

$$\mathbf{C} = \begin{pmatrix} C_{11} & C_{12} & C_{13} & C_{14} & 0 & 0 \\ C_{12} & C_{11} & C_{13} & -C_{14} & 0 & 0 \\ C_{13} & C_{13} & C_{33} & 0 & 0 & 0 \\ C_{14} & -C_{14} & 0 & C_{44} & 0 & 0 \\ 0 & 0 & 0 & 0 & C_{44} & C_{14} \\ 0 & 0 & 0 & 0 & C_{14} & C_{66} \end{pmatrix} \tag{7}$$

provided that the z axis is taken along the trigonal axis. Here, only 6 elements are independent and $C_{66} = \frac{1}{2}[C_{11} - C_{12}]$. In order to compute these elements, we consider six sets of deformations parametrized by η

$$\begin{aligned} &\eta_1 = (\eta,\eta,\eta,0,0,0) \quad ;\eta_2 = (\eta,0,0,0,0,0) \;\; ;\eta_3 = (0,0,\eta,0,0,0) \\ &\eta_4 = (0,0,0,2\eta,0,0) \;\; ;\eta_5 = (\eta,\eta,0,0,0,0) \;\; ;\eta_6 = (\eta,0,0,2\eta,0,0), \end{aligned} \tag{8}$$

where η is varied between -0.01 and 0.01 with a step of 0.001. For each deformation labelled by i and each value of η, we build the Lagrangian strain matrix η and solve Eq. 4 in an iterative way to obtain the matrix ϵ. Thus, we generate a distorted cell from the undistorted

Final draft post-refeering (pre-proofs)

one by using the matrix ϵ and we compute the total energy $E_i(\eta) \equiv E[\eta_i]$ of the distorted structure where the atomic positions are fully relaxed. Then, the energy per unit volume is fitted by a polynomial of order 4

$$\frac{E_i(\eta)}{V_0} = \sum_{j=0}^{4} A_j^i \eta^j, \tag{9}$$

where $A_0^i = E_0/V_0$, $A_1^i = 0$ and A_2^i can be expressed as a function of the unknown second order elastic constants as

$$\begin{aligned} &A_2^1 = C_{11} + C_{12} + 2C_{13} + \tfrac{1}{2}C_{33} \;; A_2^2 = \tfrac{1}{2}C_{11} \;; A_2^3 = \tfrac{1}{2}C_{33} \\ &A_2^4 = 2C_{44} \;; A_2^5 = C_{11} + C_{12} \;; A_2^6 = \tfrac{1}{2}C_{11} + 2C_{14} + 2C_{44} \end{aligned} \tag{10}$$

by using Eq. 6 and 7. The computed total energy per unit cell at 0 K including SOI (circles) together with the polynomial fit (full lines) are displayed in Fig. 1 for the two deformations respectively labelled η_3 ($a_\parallel$ varies while keeping $a_\perp$ constant) and η_5 ($a_\perp$ varies while keeping $a_\parallel$ constant). The elastic constant $C_{33}/2$ (see Fig. 1.a) is roughly four times smaller than

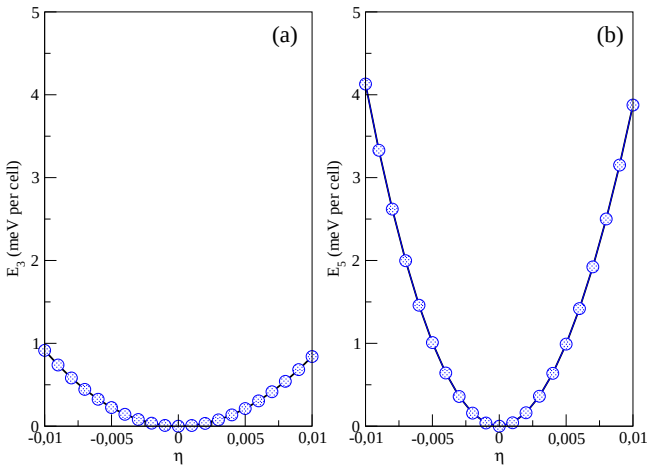

FIG. 1. Energy per unit cell (in meV) as a function of η (dimensionless quantity) for the deformations respectively labelled η_3 (Left panel) and η_5 (Right panel). The circles denote the results of the LDA calculations including SOI whereas the full lines are the result of the polynomial fit according to Eq. 9. The zero of energy corresponds to the energy of the fully relaxed structure (unstrained reference structure of volume V_0).

$C_{11}+C_{12}$ (see Fig. 1.b), reflecting the fact that bismuth is much softer against a strain along

Final draft post-refeering (pre-proofs)

TABLE II. Calculated LDA elastic constants with and without SOI of Bi compared to the experimental results at 4.2 K of Ref.[34].

	C_{11} (GPa)	C_{12} (GPa)	C_{13} (GPa)	C_{14} (GPa)	C_{33} (GPa)	C_{44} (GPa)
Experiment[34]	69.3	24.5	25.4	8.40	40.4	13.5
Present work (without SOI)	84.6	30.2	27.9	9.8	46.1	16.0
Present work (with SOI)	67.7	25.0	24.3	5.9	40.6	8.7

the trigonal axis than against a strain perpendicular to it. We do not show the energy per unit cell for the four remaining deformations but compare in Table II our calculated elastic constants with and without SOI to the experimental elastic constants indirectly obtained from the measurements of ultrasonic wave velocities by the pulse echo technique[34]. The calculated elastic constants without SOI are all overestimated with respect to experiments. Taking into account SOI leads to a decrease of all elastic constants that can be explained in a very qualitative way as follows: SOI mixes bonding and antibonding states and not only increases the equilibrium volume by 2.9 % (see Table I) but also softens the elastic constants by as much as 45 % (the larger effect being for C_{44}). As shown in Table II, the overall agreement between theory and experiment is significantly improved when SOI is included. The only exceptions are the C_{14} and C_{44} elastic constants which are underestimated by about 30% with respect to experiment. Such a discrepancy might be ascribed to experimental uncertainties associated with the sample and its bonded transducer and/or to long range effects, like van der Waals interactions, not captured by the LDA exchange-correlation functional[35]. It is also worth mentioning that all the calculated elastic constants with or without SOI satisfy Born's mechanical stability for a rhomboehedral structure[36,37] ensuring that bismuth is stable at 0 K.

Inverting the matrix **C** defined in Eq. 7 leads to the following expression for the compliance matrix :

$$\mathbf{S} = \begin{pmatrix} S_{11} & S_{12} & S_{13} & S_{14} & 0 & 0 \\ S_{12} & S_{11} & S_{13} & -S_{14} & 0 & 0 \\ S_{13} & S_{13} & S_{33} & 0 & 0 & 0 \\ S_{14} & -S_{14} & 0 & S_{44} & 0 & 0 \\ 0 & 0 & 0 & 0 & S_{44} & 2S_{14} \\ 0 & 0 & 0 & 0 & 2S_{14} & S_{66} \end{pmatrix} \tag{11}$$

Final draft post-refeering (pre-proofs)

TABLE III. Hydrostatic compressibilities χ, $\chi_{\parallel}$ and $\chi_{\perp}$ of Bi (in MBar^{-1}) obtained by using the elastic constants computed with and without SOI (see Table II) compared to the values inferred from the experimental results at 4.2 K of Ref.[34]. The ratio $\chi_{\parallel}/\chi_{\perp}$ is also given to quantify the anisotropy of the elastic properties of Bi.

	χ	$\chi_{\parallel}$	$\chi_{\perp}$	$\chi_{\parallel}/\chi_{\perp}$
Experiment[34]	2.92	1.72	0.60	2.86
Present work (without SOI)	2.55	1.58	0.49	3.24
Present work (with SOI)	2.97	1.71	0.63	2.71

where $S_{66} = 2(S_{11} - S_{12})$. The anisotropy in the elastic properties of Bi can be ascertained by introducing a parallel and a perpendicular compressibility respectively defined as

$$\chi_{\parallel} = -\frac{\partial \epsilon_{33}}{\partial P} = 2S_{13} + S_{33} = (-2C_{13} + C_{11} + C_{12})/M \tag{12}$$

and

$$\chi_{\perp} = -\frac{\partial \epsilon_{11}}{\partial P} = -\frac{\partial \epsilon_{22}}{\partial P} = S_{11} + S_{12} + S_{13} = (C_{33} - C_{13})/M, \tag{13}$$

where $M = C_{33}(C_{11} + C_{12}) - 2C_{13}^2$. The computed values of $\chi_{\parallel}$ and $\chi_{\perp}$ with and without SOI are reported in Table III. The compressibilities are underestimated with respect to experiments when SOI is neglected. Taking into account SOI leads to a very good agreement between the theoretical and experimental compressibilities in accordance with the fact that the elastic constants that play a role in the compressibilities are much better described when SOI is included (see Table II). The ratio of linear compressibilities $\chi_{\parallel}/\chi_{\perp}$ calculated when SOI is included indicates that the contraction along the trigonal axis is about 2.7 times larger than the contraction perpendicular to it upon applying an hydrostatic pressure. As stated before and illustrated in Fig. 1, Bi is stiffer perpendicularly to the trigonal axis than parallel to it. The bulk modulus B that measures material's resistance to uniform compression is defined as $B = -V_0 \frac{\partial P}{\partial V} = 1/\chi$ where the hydrostatic compressibility χ is defined as $\chi = \chi_{\parallel} + 2\chi_{\perp}$. Using the values of $\chi_{\parallel}$ and $\chi_{\perp}$ reported in Table III, we obtain a theoretical value of 33.65 (39.15) GPa for the bulk modulus B when the SOI is included (neglected). Thus, the theoretical value including the SOI agrees well with the experimental value of 34.23 GPa at 4 K[34]. All the forthcoming calculations include SOI.

Final draft post-refeering (pre-proofs)

V. THERMAL EXPANSION

We now present an analysis of the thermal expansion of bismuth using Grüneisen's theory. We follow the approach of Schelling and Keblinski[26] and emphasize the differences in the formalism used to treat the thermal expansion in anisotropic and cubic solids. Since bismuth is an anisotropic solid, the thermal expansion can be described in terms of the 3×3 thermal expansion tensor α whose components are written in terms of the strain tensor ϵ as

$$\alpha_{ab} = \left(\frac{\partial \epsilon_{ab}}{\partial T}\right)_{\sigma} \tag{14}$$

where T is the temperature and where the subscript σ means that the temperature derivative is taken at constant stress. According to the generalized form of Hookes' law, we have:

$$\epsilon_{ab} = \sum_{de} S_{abde}\sigma_{de}, \tag{15}$$

where σ_{de} and S_{abde} are the stress and the compliance elastic tensor respectively. Eq. 15 can be inverted and leads to

$$\sigma_{de} = \sum_{ij} C_{deij}\epsilon_{ij}, \tag{16}$$

where C_{deij} is the stiffness elastic tensor. Thus, we have

$$\sum_{de} S_{abde}C_{deij} = \delta_{ai}\delta_{bj} \tag{17}$$

By differentiating Eq. 17 with respect to T and by using Eq. 15 and 16, it is straightforward to show that the components of α can be written as

$$\alpha_{ab} = -\sum_{de}\left(\frac{\partial \epsilon_{ab}}{\partial \sigma_{de}}\right)_{T} \times \left(\frac{\partial \sigma_{de}}{\partial T}\right)_{\epsilon}, \tag{18}$$

where the temperature derivative of the stress tensor is taken at constant strain. This equation generalizes the expression

$$\alpha = \frac{1}{3B}\left(\frac{\partial P}{\partial T}\right)_{V} \tag{19}$$

defining the thermal expansion coefficient α of a cubic solid as a function of the bulk modulus B and the partial derivative of the pressure with respect to temperature at constant volume. The stress tensor σ_{de} appearing in Eq. 18 is defined as

$$\sigma_{de} = \frac{1}{V_0}\frac{\partial F}{\partial \epsilon_{de}} \tag{20}$$

Final draft post-refeering (pre-proofs)

where F is the Helmholtz free energy per unit cell of the crystal defined as

$$F[\epsilon] = E[\epsilon] + F_{vib}[\epsilon, T] = E[\epsilon] + \frac{1}{N}\sum_{\mathbf{q},\lambda}\frac{\hbar\omega_\lambda(\mathbf{q})}{2} + k_B T\frac{1}{N}\sum_{\mathbf{q},\lambda}\ln\left[1 - \exp\left(-\frac{\hbar\omega_\lambda(\mathbf{q})}{k_B T}\right)\right] \quad (21)$$

where the electron entropy is discarded and the vibrational contribution $F_{vib}[\epsilon, T]$ is computed within the harmonic approximation. Here, $\omega_\lambda(\mathbf{q})$ is the frequency of the phonon mode $(\mathbf{q}, \lambda)$ corresponding to wavevector $\mathbf{q}$ and polarization λ and N is the number of qpoints included in the summation. Hence, combining Eq. 20 and Eq. 21 leads to

$$\sigma_{de} = \frac{1}{V_0}\left[\frac{\partial E}{\partial \epsilon_{de}} - \frac{1}{N}\sum_{\mathbf{q},\lambda}\gamma^{de}_{\mathbf{q},\lambda}\hbar\omega_\lambda(\mathbf{q})\left(n_{\mathbf{q},\lambda} + \frac{1}{2}\right)\right], \quad (22)$$

where $n_{\mathbf{q},\lambda}$ is the Bose occupation factor at temperature T for a phonon with frequency $\omega_\lambda(\mathbf{q})$ and $\gamma^{de}_{\mathbf{q},\lambda}$ is a generalized mode Grüneisen parameter given by

$$\gamma^{de}_{\mathbf{q},\lambda} = -\frac{\partial \ln \omega_\lambda(\mathbf{q})}{\partial \epsilon_{de}} \quad (23)$$

Note that σ_{de} is temperature dependent because of the second term in Eq. 22 and that $\sigma_{de}(T \to 0)$ is renormalized by zero point atomic motions. By derivating Eq. 22 with respect to temperature T at constant strain ϵ, we get

$$\left(\frac{\partial \sigma_{de}}{\partial T}\right)_\epsilon = -\sum_{\mathbf{q},\lambda}\gamma^{de}_{\mathbf{q},\lambda}C_{\mathbf{q},\lambda} \quad (24)$$

where

$$C_{\mathbf{q},\lambda} = \frac{1}{N}\frac{\hbar\omega_\lambda(\mathbf{q})}{V_0}\left(\frac{\partial n_{\mathbf{q},\lambda}}{\partial T}\right)_\epsilon \quad (25)$$

is the contribution of mode $(\mathbf{q}, \lambda)$ to the lattice specific heat per unit volume at constant volume C_V. Thus C_V is given by

$$C_V(T) = \sum_{\mathbf{q},\lambda} C_{\mathbf{q},\lambda} = \frac{k_B}{V_0}\frac{1}{N}\sum_{\mathbf{q},\lambda}\left(\frac{\hbar\omega_\lambda(\mathbf{q})}{2k_B T}\right)^2 \frac{1}{\sinh^2\left(\frac{\hbar\omega_\lambda(\mathbf{q})}{2k_B T}\right)}. \quad (26)$$

Finally, by using Eq. 15 and inserting Eq. 24 in Eq. 18, we obtain

$$\alpha_{ab} = \sum_{\mathbf{q},\lambda} C_{\mathbf{q},\lambda}\sum_{de} S_{abde}\gamma^{de}_{\mathbf{q},\lambda}. \quad (27)$$

In a completely harmonic lattice, the frequencies would be independent of the strain and the $\gamma^{de}_{\mathbf{q},\lambda}$ would be zero, leading to a zero thermal expansion. Eq. 27 generalizes the expression

$$\alpha = \frac{1}{3B}\sum_{\mathbf{q},\lambda} C_{\mathbf{q},\lambda}\gamma_{\mathbf{q},\lambda}, \quad (28)$$

Final draft post-refeering (pre-proofs)

giving the thermal expansion coefficient α for a cubic solid. Here $C_{\mathbf{q},\lambda}$ is defined in Eq. 25 and $\gamma_{\mathbf{q},\lambda}$ is the mode Grüneisen parameter defined as

$$\gamma_{\mathbf{q},\lambda} = -\partial \ln[\omega_\lambda(\mathbf{q})]/\partial \ln V. \tag{29}$$

Usually, the phonon frequencies $\omega_\lambda(\mathbf{q})$ decrease as the volume V increases giving rise to positive Grüneisen parameters and thus to a positive thermal expansion coefficient α at any temperature as can be inferred from Eq. 28. Inserting the non-zero matrix elements of $\mathbf{S}$ allowed by symmetry (see Eq. 11) in Eq. 27 and taking into account the fact that $\gamma^{de}_{\mathbf{q},\lambda} = 0$ when $d \neq e$ leads to the following expressions

$$\alpha_\perp \equiv \alpha_{11} \equiv \alpha_{22} = \sum_{\mathbf{q},\lambda} C_{\mathbf{q},\lambda} \left[(S_{11} + S_{12})\, \gamma^{\perp}_{\mathbf{q},\lambda} + S_{13} \gamma^{\parallel}_{\mathbf{q},\lambda} \right] \tag{30}$$

and

$$\alpha_\parallel \equiv \alpha_{33} = \sum_{\mathbf{q},\lambda} C_{\mathbf{q},\lambda} \left[2S_{13} \gamma^{\perp}_{\mathbf{q},\lambda} + S_{33} \gamma^{\parallel}_{\mathbf{q},\lambda} \right] \tag{31}$$

where $\alpha_\perp$ and $\alpha_\parallel$ are the thermal expansion coefficient respectively within the basal plane and along the ternary axis. Here,

$$\gamma^{\perp}_{\mathbf{q},\lambda} \equiv \frac{1}{2} \left(\gamma^{11}_{\mathbf{q},\lambda} + \gamma^{22}_{\mathbf{q},\lambda} \right) = -\frac{a_{\perp,0}}{2\omega^0_\lambda(\mathbf{q})} \frac{\partial \omega_\lambda(\mathbf{q})}{\partial a_\perp} \tag{32}$$

and

$$\gamma^{\parallel}_{\mathbf{q},\lambda} \equiv \gamma^{33}_{\mathbf{q},\lambda} = -\frac{a_{\parallel,0}}{\omega^0_\lambda(\mathbf{q})} \frac{\partial \omega_\lambda(\mathbf{q})}{\partial a_\parallel} \tag{33}$$

where $a_{\perp,0}$ and $a_{\parallel,0}$ are the LDA lattice parameters reported in Table I and $\omega^0_\lambda(\mathbf{q})$ are the phonon frequencies calculated for these lattice parameters. We do not compare our computed $\omega^0_\lambda(\mathbf{q})$ with available experimental data because the agreement between theory and experiments has already been highlighted in a thorough study based on calculations performed using the ABINIT code[33]. A finite difference scheme based on a relative variation of ± 0.2 % of $a_\perp$ and $a_\parallel$ around $a_{\perp,0}$ and $a_{\parallel,0}$ is used to compute the partial derivatives of the phonon frequencies $\omega_\lambda(\mathbf{q})$ with respect to $a_\perp$ and $a_\parallel$. Hence, the mode Grüneisen parameters respectively defined in Eq. 32 and Eq. 33 are computed for a $32 \times 32 \times 32$ qpoints grid and for all polarizations λ.

The Figure. 2 shows that the mode Grüneisen parameters $\gamma^{\parallel}_{\mathbf{q},\lambda}$ and $\gamma^{\perp}_{\mathbf{q},\lambda}$ are rather scattered for the acoustic modes with quite large positive values but also negative values. About 40 % and 18 % of the mode Grüneisen parameters are negative for the first and second

Final draft post-refeering (pre-proofs)

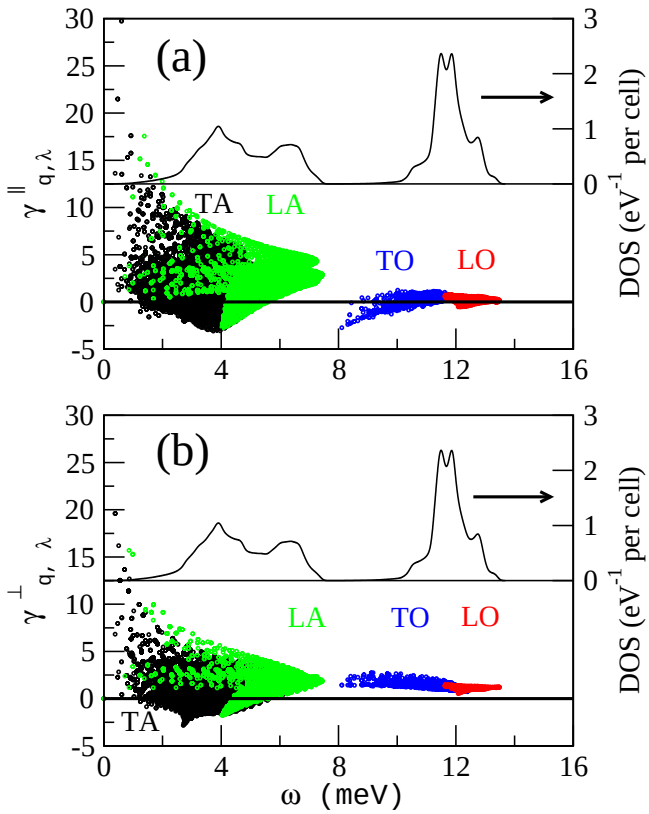

FIG. 2. Calculated Grüneisen parameters $\gamma^{\parallel}_{\mathbf{q},\lambda}$ and $\gamma^{\perp}_{\mathbf{q},\lambda}$ as a function of phonon energy ω in meV (Left vertical scale) together with the phonon density of states (Right vertical scale).

transverse acoustic branch (TA) while less than 5 % of the mode Grüneisen parameters are negative for the longitunal acoustic branch (LA).

By comparing Figs 2(a) and 2(b), we note that the mode Grüneisen parameters $\gamma^{\parallel}_{\mathbf{q},\lambda}$ are slightly larger than the mode Grüneisen parameters $\gamma^{\perp}_{\mathbf{q},\lambda}$ for acoustic modes with energy ranging from 0 to 7.5 meV (TA+LA). On the contrary, the mode Grüneisen parameters $\gamma^{\parallel}_{\mathbf{q},\lambda}$ are almost 3 times smaller in average than the mode Grüneisen parameters $\gamma^{\perp}_{\mathbf{q},\lambda}$ for optical modes with energy ranging from 8 to 13.5 meV (TO+LO). In other words, the optical phonon frequencies are more sensitive to a variation of $a_{\perp}$ than to a variation of $a_{\parallel}$ while the opposite is true for the acoustic phonon frequencies.

We can also introduce macroscopic Grüneisen functions

$$\gamma^{\perp,\parallel} = \left(\sum_{\mathbf{q},\lambda} \gamma^{\perp,\parallel}_{\mathbf{q},\lambda} C_{\mathbf{q},\lambda} \right) / C_V \tag{34}$$

Final draft post-refeering (pre-proofs)

where $C_{\mathbf{q},\lambda}$ and C_V are respectively defined in Eq. 25 and 26. The calculated lattice specific heat at constant volume C_V displayed in Fig. 3(a) is in good agreement with the experimental lattice specific heat at constant pressure up to the Debye temperature $\theta_D = 119$ K[41]. As shown in Fig. 3(b), the behaviour of the temperature dependent Grüneisen functions $\gamma^{\perp}$ and $\gamma^{\parallel}$ is quite complex with a crossover around 40 K. However, $\gamma^{\perp}$ and $\gamma^{\parallel}$ saturate towards

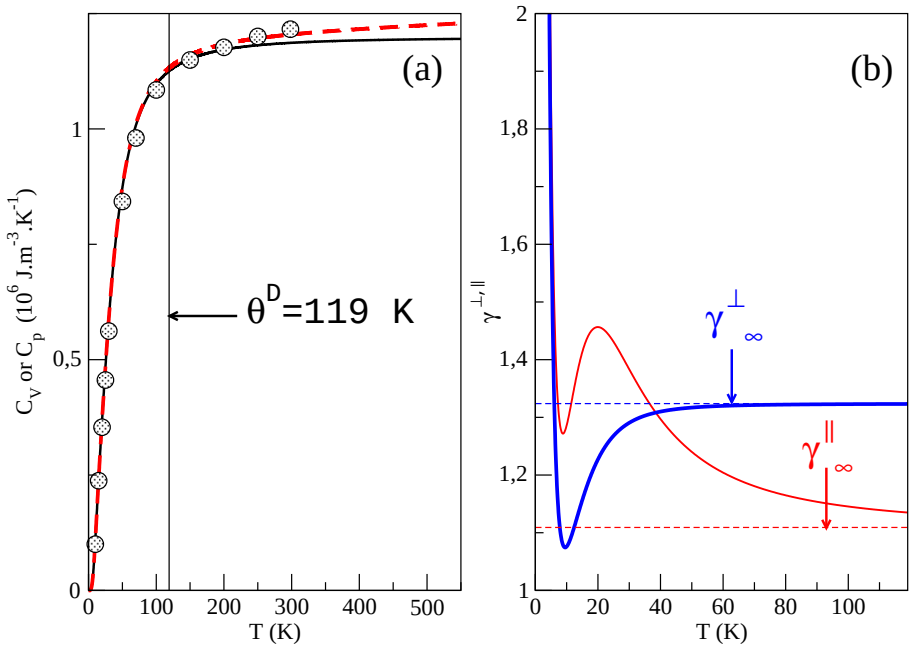

FIG. 3. (a) Calculated lattice specific heat per unit volume at constant volume C_V (solide curve) or at constant pressure C_p (dashed curve) compared to experimental data (open circles) from Ref.[41] for temperatures T up to the melting temperature of 545 K. (b) Grüneisen functions $\gamma^{\perp,\parallel}$ as a function of temperature T up to the Debye temperature θ_D of 119 K[41].

$\gamma^{\perp}_{\infty} = 1.32$ and $\gamma^{\parallel}_{\infty} = 1.11$ when $T \gg \theta_D$ in accordance with the fact that

$$\lim_{T\to\infty} \gamma^{\perp,\parallel}(T) = \frac{1}{6N}\sum_{\mathbf{q},\lambda} \gamma^{\perp,\parallel}_{\mathbf{q},\lambda}, \tag{35}$$

since $C_{\mathbf{q},\lambda}(T) \to k_B/V_0 N$ and $C_V(T) \to 6k_B/V_0$ when $T \to \infty$. Interestingly, the high temperature limiting values of $\gamma^{\perp}_{\infty}$ and $\gamma^{\parallel}_{\infty}$ extracted from experimental results[38] are estimated to be 1.32 and 1.10 and are in excellent agreement with our calculated values.

Following the approach of Munn[40], the principal coefficients of thermal expansion defined

Final draft post-refeering (pre-proofs)

in Eq. 30 and 31 can also be expressed as

$$\alpha_{\perp} = C_V \left[\chi_{\perp}\gamma^{\perp} + S_{13}\left(\gamma^{\parallel} - \gamma^{\perp}\right)\right] \tag{36}$$

$$\alpha_{\parallel} = C_V \left[\chi_{\parallel}\gamma^{\parallel} - 2S_{13}\left(\gamma^{\parallel} - \gamma^{\perp}\right)\right] \tag{37}$$

where the directional Grüneisen functions $\gamma^{\perp,\parallel}$ are defined in Eq. 34 and the compressibilities $\chi_{\parallel}$ and $\chi_{\perp}$ are respectively defined in Eq. 12 and 13. It is a good first approximation to treat both the compressibilities and the compliance matrix element S_{13} as constant, and regard the temperature dependence of the coefficients of thermal expansion as due solely to that of the heat capacity C_V and the Grüneisen functions $\gamma^{\perp,\parallel}$. Such expressions for the coefficients of thermal expansion allow to disentangle the role of the anisotropy in either the Grüneisen functions or the elastic constants. Fig. 3(b) shows that $\gamma^{\parallel} = \gamma^{\perp}$ for T=40 K. Thus, the anisotropy in the thermal expansion coefficients measured by $\alpha_{\parallel}/\alpha_{\perp}$ is given by $\chi_{\parallel}/\chi_{\perp} = 2.71$ (see Table III) and is only due to the anisotropy in the elastic properties. When moving away from the crossover temperature (T=40 K), the term proportionnal to $\gamma^{\parallel} - \gamma^{\perp}$ starts to play a role as the cross-compliance $S_{13} = -C_{13}/M$ ($\sim$ -0.94 MBar^{-1}) has the same order of magnitude as $\chi_{\parallel}$ and $\chi_{\perp}$ (see Table III). For $\alpha_{\parallel}$, the correction arising from the anisotropy in the Grüneisen functions is given by $-2C_V S_{13}\left(\gamma^{\parallel} - \gamma^{\perp}\right)$ and remains very small at low temperature since $C_V \to 0$ when $T \to 0$. Thus, the correction is small and positive for $T < 40$ K since $S_{13} < 0$ and $\gamma^{\parallel} - \gamma^{\perp} > 0$ in this low temperature regime. However, the correction becomes non negligible at higher temperatures and negative as the sign of $\gamma^{\parallel} - \gamma^{\perp}$ changes when $T > 40$ K. The high temperature limit of this correction is given by $-12k_B S_{13}(\gamma^{\parallel}_{\infty} - \gamma^{\perp}_{\infty})/V_0$ and is sketched as a vertical downward arrow in Fig. 4. For $\alpha_{\perp}$, the same type of conclusion holds but the sign and the magnitude of the correction is changed since it is given by $C_V S_{13}\left(\gamma^{\parallel} - \gamma^{\perp}\right)$. The high temperature limit of this correction is given by $6k_B S_{13}(\gamma^{\parallel}_{\infty} - \gamma^{\perp}_{\infty})/V_0$ and is depicted as a vertical upward arrow in Fig. 4 since this quantity is positive. The thermal expansion coefficients parallel ($\alpha_{\parallel}$) and perpendicular ($\alpha_{\perp}$) to the ternary axis calculated neglecting (dashed curves) and including (full curves) the anisotropy in the Grüneisen functions are displayed in Fig. 4. At low temperature ($T < 40$ K), the anisotropy in the Grüneisen functions plays a minor role since the full curves almost coincide with the dashed curves. However, it starts to contribute at higher temperature since it reduces $\alpha_{\parallel}$ and increases $\alpha_{\perp}$ significantly, thereby reducing the anisotropy in the thermal expansion coefficients given by $\alpha_{\parallel}/\alpha_{\perp}$ and bringing our calculated

Final draft post-refeering (pre-proofs)

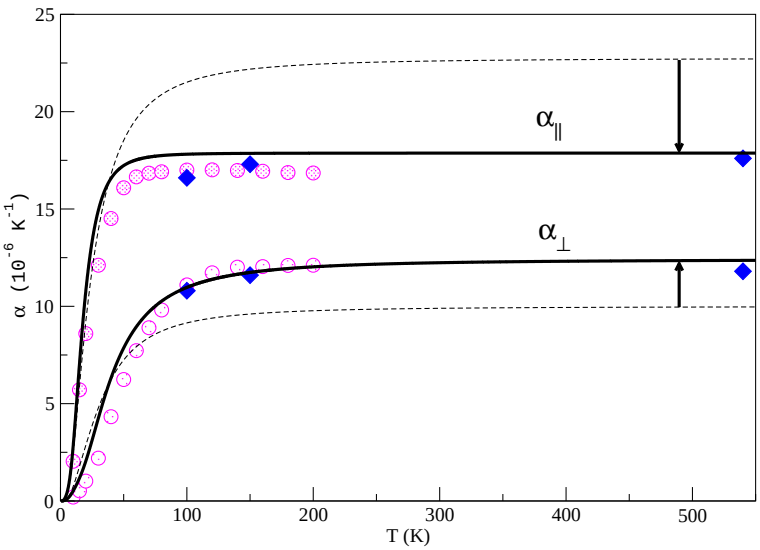

FIG. 4. Coefficient of linear thermal expansion of bismuth within the basal plane ($\alpha_\perp$) and along the ternary axis ($\alpha_\parallel$) as a function of temperature T up to the melting temperature. Experimental data are denoted by circles[38] and losanges[39]. The full curves are calculated using Eq. 36 and 37 while the dashed curves are calculated by neglecting the anisotropy in the Grüneisen functions, which is tantamount to put $S_{13} = 0$ in Eq. 36 and 37.

thermal expansion coefficients in closer agreement with the measurements made using an optical lever dilatometer[38,39]. Thus, the quasi-harmonic approximation based on quantities calculated at 0 K provides quite accurate results compared to experimental data[38,39], even near the melting temperature of bismuth where renormalization effects due to the temperature dependence of elastic constants might be important[24] and where the applicability of the quasiharmonic approximation is also questionable because large anharmonic effects are expected. It's worth coming back to the calculated lattice specific heat at constant volume C_V shown in Fig. 3(a). Above θ_D, the experimental lattice specific heat at constant pressure deviates from C_V and should in principle be compared to C_p. A very simple reasoning based on thermodynamics[42] shows that

$$C_p - C_V = \alpha^2 BT, \tag{38}$$

where $\alpha \equiv \frac{1}{V_0}\left(\frac{\partial V}{\partial T}\right)_P = \alpha_\parallel + 2\alpha_\perp$ is the volumetric expansion coefficient and B is the temperature dependent bulk modulus, which can be approximated by it's 0 K value. The

Final draft post-refeering (pre-proofs)

calculated C_p displayed in Fig. 3(a) coincides with the calculated C_V below the Debye temperature θ_D because $\alpha(T) \to 0$ when $T \ll \theta_D$, making the correction $\alpha^2 BT$ very small in this temperature range. When $T > \theta_D$, $\alpha(T)$ becomes constant and the correction increases linearly with T. The agreement between theory and experiment is improved since all the experimental data (open circles) collapse on the calculated C_p (dashed curve) up to room temperature.

VI. CONCLUSION

We performed first-principles calculations in order to understand the anisotropic thermal expansion of bismuth. First, we computed the elastic constants of bismuth at 0 K using a finite strain approach. All the elastic constants, with the exception of the C_{14} and C_{44} elastic constants, are found to be in good agreement with experimental results[34] when the SOI is included. We also calculated the hydrostatic compressibilities along the ternary axis ($\chi_\parallel$) and perpendicular to it ($\chi_\perp$) and found that the anisotropy in the directional compressibilities is large since $\chi_\parallel/\chi_\perp \sim 2.7$. Then, we computed the thermal expansion coefficients parallel ($\alpha_\parallel$) and perpendicular ($\alpha_\perp$) to the ternary axis using the quasiharmonic approximation. These quantities are found to be in close agreement with experiments[38,39]. Another outcome of our calculations is that the anisotropy in the thermal expansion coefficients is essentially governed by the anisotropy in the mechanical properties below the Debye temperature θ_D while both the anisotropy in the directional compressibilities and in the directional Grüneisen functions play a role at higher temperatures. Finally, this work is a first step towards a first-principles description of the thermal/non thermal expansion in laser-excited bismuth[20], where the electron system is not equilibrated with the phonon system[17,18].

ACKNOWLEDGMENTS

Calculations were performed using HPC resources from GENCI-CINES (project 095096).

[1] P. B. Alers and R. T. Webber, Phys. Rev. **91**, 1060 (1953).

Final draft post-refeering (pre-proofs)

[2] Xu Du, Shan-Wen Tsai, Dmitrii L. Maslov, and Arthur F. Hebard, Phys. Rev. Lett. **94**, 166601 (2005).

[3] R. W. Boydston, Phys. Rev. **30**, 911 (1927).

[4] B.S. Chandrasekhar, Journal of Physics and Chemistry of Solids **11**, 268 (1959).

[5] Y. Fuseya, M. Ogata and H. Fukuyama, J. Phys. Soc. Jpn. **84**, 012001 (2015).

[6] Ph. Hofmann, Prog. Surf. Sci. **81**, 191 (2006).

[7] K. S. Novoselov, S. V. Morozov, S. V. Dubonos, M. Missous, A. O. Volkov, D. A. Christian, and A. K. Geim, J. Appl. Phys. **93**, 10053 (2003).

[8] J. Kokorian, J.B.C. Engelen, J. de Vries, H. Nazeer, L.A. Woldering, L. Abelmann, Thin Solid Films **550**, 298 (2014).

[9] K. Sokolowski-Tinten *et al.*, Nature **422**, 287 (2003).

[10] D.M. Fritz *et al*, Science **315**, 633 (2007).

[11] S.L. Johnson *et al.*, Phys. Rev. Lett. **100**, 155501 (2008).

[12] S.L. Johnson *et al.*, Phys. Rev. Lett. **102**, 175503 (2009).

[13] E. Papalazarou, J. Faure, J. Mauchain, M. Marsi, A. Taleb-Ibrahimi, I. Reshetnyak, A. van Roekeghem, I. Timrov, N. Vast, B. Arnaud, and L. Perfetti, Phys. Rev. Lett. **108**, 256808 (2012).

[14] J. Faure, J. Mauchain, E. Papalazarou, M. Marsi, D. Boschetto, I. Timrov, N. Vast, Y. Ohtsubo, B. Arnaud, and L. Perfetti, Phys. Rev. B **88**, 075120 (2013).

[15] E.D. Murray, D.M. Fritz, J.K. Wahlstrand, S. Fahy and D.A. Reis, Phys. Rev. B **72**, 060301 (2005).

[16] E. S. Zijlstra, L. L. Tatarinova, and M. E. Garcia, Phys. Rev. B **74**, 220301 (2006).

[17] Y. Giret, A. Gellé and B. Arnaud, Phys. Rev. Lett. **106**, 155503 (2011).

[18] B. Arnaud and Y. Giret, Phys. Rev. Lett. **110**, 016405 (2013).

[19] E. D. Murray and S. Fahy, Phys. Rev. Lett. **114**, 055502 (2015).

[20] C. Laulhé, M. Cammarata, M. Servol, R. J. Dwayne Miller, M. Hada, S. Ravy, Eur. Phys. J. Special Topics **222**, 1277 (2013).

[21] P. Giannozzi, S. de Gironcoli, P. Pavone and S. Baroni, Phys. Rev. B. **43**, 7231 (1991).

[22] A. Debernardi and M. Cardona, Phys. Rev. B. **54**, 11305 (1996).

[23] B. B. Karki, R. M. Wentzcovitch, S. de Gironcoli, S. Baroni, Science. **286**, 1705 (1999).

[24] A. Debernardi, M. Alouani, and H. Dreyssé, Phys. Rev. B **63**, 064305 (2001).

Final draft post-refeering (pre-proofs)

[25] A. I. Lichtenstein, R. O. Jones, H. Xu, and P. J. Heaney, Phys. Rev. B. **58**, 6219 (1998).

[26] P. K. Schelling and P. Keblinski, Phys. Rev. B **68**, 035425 (2003).

[27] N. Mounet and N. Marzari, Phys. Rev. B. **71**, 205214 (2005).

[28] S. Q. Wang, Appl. Phys. Lett.. **88**, 061902 (2006).

[29] X. Gonze *et al*, Comput. Phys. Commun. **180**, 2582 (2009).

[30] S. Goedecker, M. Teter and J. Hutter, Phys. Rev. B **54**, 1703 (1996).

[31] X. Gonze, Phys. Rev. B **55**, 10337 (1997).

[32] P. Cucka, C.S. Barrett, Acta Cryst. **15**, 865 (1962).

[33] L. E. Díaz-Sánchez, A. H. Romero, and X. Gonze, Phys. Rev. B **76**, 104302 (2007).

[34] A. J. Lichnowski and G. A. Saunders, J. Phys. C, **9**, 927 (1976).

[35] Tomáš Bučko, S. Lebègue, Jürgen Hafner, and J. G. Ángyán, Phys. Rev. B, **87**, 064110 (2013).

[36] M. Born, Math. Proc. Camb. Phil. Soc. **36**, 160 (1940).

[37] F. Mouhat and F.X. Coudert, Phys. Rev. B, **90**, 224104 (2014).

[38] G. V. Bunton and S. Weintroub, J. Phys. C: Solid State Phys. **2**, 116 (1969).

[39] E. F. Cave and L. V. Holroyd, J. Appl. Phys. **31**, 1357 (1960).

[40] R. W. Munn, J. Phys. C: Solid State Phys. **5**, 535 (1972).

[41] D.E. Gray *et al*, American institute of Physics Handbook, 3rd ed., McGraw-Hill Book Company.

[42] H. Callen, *Thermodynamic* (Wiley and Sons, New York, 1960).

Final draft post-refeering (pre-proofs)